

9A.5 AN IMMERSSED BOUNDARY METHOD FOR FLOW OVER COMPLEX TERRAIN

Katherine A. Lundquist^{1,2,*}, Fotini K. Chow¹, and Julie K. Lundquist²

¹ University of California, Berkeley, CA

² Lawrence Livermore National Laboratory, Livermore, CA

1 INTRODUCTION

Most mesoscale numerical models use terrain-following coordinates to accommodate complex terrain. Terrain-following or sigma coordinates conform to the bottom topography and the coordinate lines gradually become smoother and flatter with distance from the ground. With very steep terrain, the coordinate lines retain a signature of the underlying surface shape even very far away from the ground. Coordinate transformations are introduced into the discretized equations and produce numerical truncation errors in addition to those associated with the chosen discretization scheme.

Several methods have been proposed to reduce the truncation error arising from terrain-following coordinates. Schär et al. [2002] proposed a modified sigma coordinate in which grid distortion due to small scale terrain features decays with height more rapidly than distortion caused by large scale features. The modified coordinate flattens quickly with height and improves the accuracy of the solution. Klemp et al. [2003] investigated the errors that arise when numerical treatment of the metric terms is inconsistent with the discretization of other terms in the governing equations. Distortion seen in topographically induced gravity waves was reduced with consistent numerical treatment. Adcroft et al. [1997] used a shaved cell approach to represent topography on a Cartesian grid. This method eliminates grid distortion, but introduces complications in the numerical solution at the ground because the computational cells must be modified (shaved) where they intersect the topography.

Here we introduce an alternative gridding technique for flow over complex terrain using an immersed boundary method (IBM) in the Weather Research and Forecasting (WRF) model. With this method, the terrain surface intersects the grid, and variables are adjusted near the immersed bound-

ary so that the flow is diverted by the boundary. Grid distortion and the associated truncation errors are thus avoided. Additionally, the method does not require modification of the computational stencil in the vicinity of the topography. Boundary conditions are imposed on the immersed surface for velocities and scalar quantities through interpolation. The implementation and validation of IBM in WRF in two dimensions has been described previously by Lundquist et al. [2007, 2008]. Here we focus on the behavior of the flow far above steep topography.

A description of the WRF model, its native sigma coordinate, and the alternative immersed boundary method are provided in section 2. The scalar transport test case of Schär et al. [2002] is presented in section 3. Comparisons are made between simulations using standard terrain-following coordinates and those using IBM. Large truncation errors are present in the native coordinate, and it is demonstrated that the immersed boundary method can be used within WRF to alleviate these errors. Truncation errors can be attributed to either the finite differencing scheme or the metric terms. Further analysis in section 4 apportions the error attributable to each cause.

2 NUMERICAL METHOD

Relevant details of the WRF coordinate, governing equations, and discretization are provided in this section, along with a description of the immersed boundary method. Further details of the WRF governing equations and discretization techniques are found in Klemp et al. [2007]. Skamarock et al. [2005] provides a complete description of the model, including default settings and model parameterizations.

2.1 COORDINATE DEFINITIONS

Terrain-following coordinates were first introduced by Phillips [1957] for numerical weather forecasting models using pressure as an independent variable

* *Corresponding author address:* Katherine A. Lundquist, Mechanical Engineering, 6189 Etcheverry Hall, University of California, Berkeley, 94720-1742, email: katielundquist@berkeley.edu

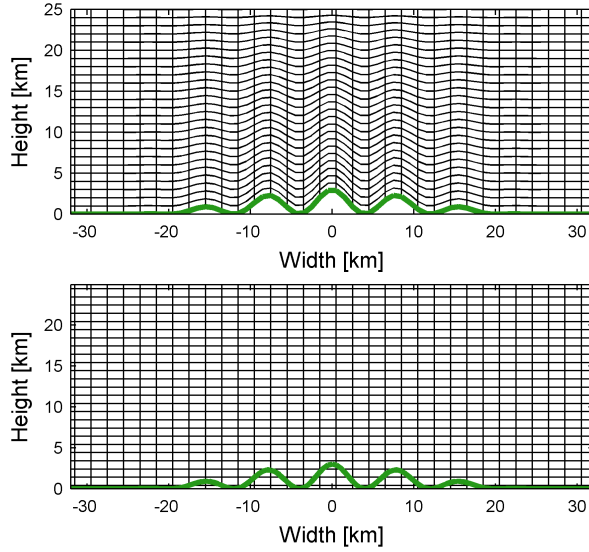


Figure 1: Terrain-following coordinates shown in the top figure, and coordinates where the immersed boundary method is used are shown in the bottom figure. These grids are used for the idealized advection test in section 3. Every other coordinate line is shown.

representing the vertical coordinate. Gal-Chen and Somerville [1975] use a height-based sigma coordinate to map non-orthogonal coordinates onto a Cartesian grid. Most modern mesoscale models employ one of these two options to accommodate terrain, both of which introduce terrain-induced grid distortion.

A pressure or mass based vertical coordinate η is used in WRF, and is given in terms of the dry hydrostatic pressure P_{hs} . The coordinate is defined such that it is zero at the top of the computational domain and unity at the terrain surface. This yields the coordinate definition $\eta = \frac{P_{hs} - P_{hs,top}}{\mu}$, where the column mass per unit area of the fluid is $\mu(x, y) = P_{hs,surface} - P_{hs,top}$. The grid used in the idealized advection test (section 3) is included in figure 1, where the η coordinate is shown in the top figure.

When the immersed boundary method is used, the grid is not transformed to align with the topography. Instead, the terrain is allowed to arbitrarily pass through the grid as shown in the bottom domain in figure 1. The effects of the solid boundaries on the fluid are represented by the addition of a body force term F_B in the conservation equations for momentum and scalars (1). Mathematically, the forcing term takes a non-zero value in the vicinity of the immersed boundary, but has no effect away

from the boundaries.

$$\partial_t \vec{V} + \vec{V} \cdot \nabla \vec{V} = -\alpha \nabla p + \nu_t \nabla^2 \vec{V} + \vec{g} + \vec{F}_B \quad (1a)$$

$$\partial_t \phi + \vec{V} \cdot \nabla \phi = \nu_t \nabla^2 \phi + F_B \quad (1b)$$

The forcing method used in this work is referred to as direct or discrete forcing, which first appeared in Mohd-Yusof [1997]. With this method the velocity or scalar value is modified at forcing points near the terrain to enforce the boundary condition, eliminating the need for explicit calculation of the body force term. Terrain passes through the grid, and a bilinear interpolation method is used to determine the forcing needed at discrete grid points. The implementation of this method in the WRF model is documented in Lundquist et al. [2007, 2008].

2.2 DETAILS OF THE WEATHER RESEARCH AND FORECASTING MODEL

The mesoscale model WRF solves the non-hydrostatic compressible Euler equations which have been transformed into a pressure-based terrain-following coordinate. Two coordinate transformations are required. The first transforms the equations into the hydrostatic pressure coordinate, and the second transforms the equations into the terrain-following coordinate. An additional velocity is introduced in these transformations, and is defined as the contravariant velocity of the vertical coordinate $\dot{\eta}$. Therefore, WRF solves the transformed Navier-Stokes equations plus an additional equation representing $\dot{\eta}$. The coordinate velocity is relevant here because the definition contains terms from the Jacobian matrix for the coordinate transformation. The equation defining $\dot{\eta}$ is rearranged so that it appears in WRF as a prognostic equation for the geopotential ϕ . The transformed equations are given in 2.

$$\partial_t \mu + \nabla \cdot (\mu \vec{V}) + \partial_\eta (\mu \dot{\eta}) = 0 \quad (2a)$$

$$\partial_t (\mu \vec{V}) + \nabla \cdot (\mu \vec{V}; \vec{V}) + \partial_\eta (\mu \dot{\eta} \vec{V}) - \nabla \cdot (p \partial_\eta \phi) + \partial_\eta (p \nabla \phi) = \vec{F} \quad (2b)$$

$$\partial_t (\mu w) + \nabla \cdot (\mu \vec{V} w) + \partial_\eta (\mu \dot{\eta} w) - g (\partial_\eta p - \mu) = F \quad (2c)$$

$$\partial_t \phi + \vec{V} \cdot \nabla \phi + \dot{\eta} \partial_\eta \phi - gw = 0 \quad (2d)$$

In the above equations \vec{V} only includes horizontal velocities, and ∇ operates on coordinate surfaces in the horizontal dimension. Geopotential is defined as $\phi = gz$, so that $\nabla \phi$ and $\partial_\eta \phi$ are surrogates for the Jacobian terms ∇z and $\partial_\eta z$.

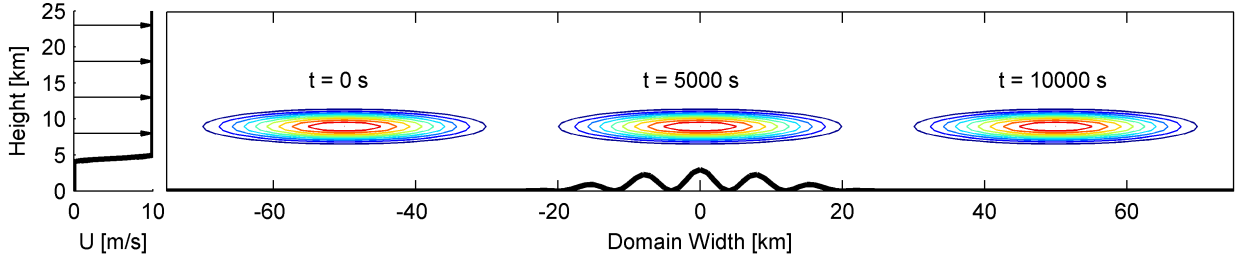


Figure 2: Set-up of the idealized advection test from Schär et al. [2002]. Topography is placed within a stagnant air mass, with uniform flow above. The analytic solution is shown for advection of a scalar cloud at three different times.

Terms created by the change of coordinates may be evaluated analytically if the terrain function is differentiable and the Jacobian matrix is invertible. Instead it is often more practical to compute the metric terms numerically, as is the case in WRF. The Jacobian maps the physical topography onto a rectangular domain, but in WRF the terms are also affected by movement of the vertical coordinate during the time integration. Therefore, the Jacobian terms appearing in WRF must be evaluated numerically at each time step. The terms are evaluated with an even-order finite difference scheme that is greater than or equal to the order of the advection scheme. If a 3rd or 4th order advection scheme is used, the Jacobian terms are evaluated with a 4th order scheme. When the immersed boundary method is used the coordinates are still changed into pressure coordinates, but the transformation to terrain-following coordinates is eliminated. Horizontal gradients of the coordinate are substantially reduced with IBM, but the magnitude of the gradients may not be exactly zero due to time variability of the grid arising from the transformation to pressure coordinates.

The governing equations are spatially discretized using an Arakawa C staggered grid. A time-split integration scheme handles the full range of frequencies admitted by the compressible Navier-Stokes equations. An explicit 3rd order Runge Kutta method is used to advance meteorologically significant low frequency modes. High frequency modes, such as acoustic waves, are integrated on a smaller time step. Horizontally propagating acoustic modes are integrated with an explicit forward-backward scheme, and vertically propagating acoustic modes and buoyancy oscillations are treated implicitly. Advection terms may be evaluated with numerical schemes ranging from 2nd to 6th order. Explicit diffusion is not used in the test case presented in this work.

3 IDEALIZED ADVECTION TEST

The idealized advection test presented in Schär et al. [2002] is used here to demonstrate the effects of truncation errors in the WRF model. In this section, truncation errors arising from both the finite-differencing scheme and the coordinate transformation are considered. It is shown that these errors are significantly reduced when the immersed boundary method is used.

For this test case, highly variable topography resides in a quiescent air mass, with a uniform horizontal flow aloft, as shown in figure 2. A shear layer in the velocity sounding persists without mixing due to the absence of viscosity. The shear layer isolates the effects of the terrain from the flow aloft, so that when a scalar anomaly is introduced it advects over the terrain without distortion or diffusion. The analytical solution for the advection of a scalar cloud is presented in figure 2 at three different times. When terrain-following coordinates are used, the horizontal grid lines retain the signature of the topographic features. Discretization of the terrain-following coordinates leads to an additional truncation error which is a function of the Jacobian. These truncation errors cause distortion of the scalar as it advects through the domain as illustrated below.

3.1 MODEL SET-UP AND INITIALIZATION

In this test, the topography is specified as the product of two oscillatory functions. The first function has a large-scale wavelength of 50 km, and the second perturbation function has a wavelength of 8km. The equation for the topography is given as 3, where $h_o = 3$ km, $a = 25$ km, and $\lambda = 8$ km.

$$h_x(x) = \begin{cases} h_o \cos^2\left(\frac{\pi x}{2a}\right) \cos^2\left(\frac{\pi x}{\lambda}\right) & \text{for } |x| \leq a \\ 0 & \text{for } |x| > a \end{cases} \quad (3)$$

Velocity, potential temperature, and water vapor mixing ratio are specified with a vertical sounding. Velocity is specified by equation 4, where $u_o = 10 \text{ m s}^{-1}$, $z_1 = 4 \text{ km}$, and $z_2 = 5 \text{ km}$.

$$u(z) = \begin{cases} u_o & \text{for } z > z_2 \\ u_o \sin^2\left(\frac{\pi}{2} \frac{z-z_1}{z_2-z_1}\right) & \text{for } z_1 \leq z \leq z_2 \\ 0 & \text{for } z < z_1 \end{cases} \quad (4)$$

The atmosphere is neutrally stable with a potential temperature of 288 K. A dry atmosphere is considered.

The total domain size is $(X, Y, Z) = (300 \text{ km}, 2 \text{ km}, 25 \text{ km})$ for the simulation with terrain following coordinates. When the immersed boundary method is used, the domain is extended 1 km in the vertical dimension to $(X, Y, Z) = (300 \text{ km}, 2 \text{ km}, 26 \text{ km})$. The vertical domain ranges from -1 km to 25 km, allowing for computational nodes below the zero terrain height. These extra nodes are used as forcing points in the immersed boundary method. The number of grid points in the terrain-following coordinate case is $(n_x, n_y, n_z) = (301, 3, 51)$, and with the immersed boundary method it is $(n_x, n_y, n_z) = (301, 3, 54)$. Horizontal resolution in the base case is $\Delta X = \Delta Y = 1 \text{ km}$, and vertical resolution is $\Delta Z = 0.5 \text{ km}$. The time step is $\Delta t = 20 \text{ s}$. Schär et al. [2002] use a 25 s time step; however, a smaller time step of 20 s is needed in WRF to achieve numerical stability.

The scalar cloud is defined by equation 5, where the maximum amplitude is $\varphi_o = 1$, the horizontal half width is $A_x = 25 \text{ km}$, and the vertical half width is $A_z = 3 \text{ km}$.

$$r = \left[\left(\frac{x - x_o}{A_x} \right)^2 + \left(\frac{z - z_o}{A_z} \right)^2 \right]^{1/2} \quad (5a)$$

$$\varphi(x, z) = \begin{cases} \varphi_o \cos^2\left(\frac{\pi r}{2}\right) & \text{for } r \leq 1 \\ 0 & \text{for } r > 1 \end{cases} \quad (5b)$$

The scalar is initialized at the location $(X_o, Z_o) = (-50 \text{ km}, 9 \text{ km})$. It is centered in the domain at $t = 5000 \text{ s}$, and the center is located at $(X_o, Z_o) = (50 \text{ km}, 9 \text{ km})$ when the time integration ends at $t = 10000 \text{ s}$.

3.2 RESULTS USING DEFAULT WRF SETTINGS

A comparison is made between two WRF simulations, the first with the native terrain-following coordinates, and the second with the newly implemented immersed boundary method. Default WRF options are used, and include a 3rd order Runge

Kutta time stepping scheme, 5th order horizontal advection, and 3rd order vertical advection. The odd-order advection schemes are upwind-biased and diffusive. Default constants are used for filtering in time, and include a divergence damping coefficient $\gamma_d = 0.1$, external mode damping coefficient $\gamma_e = 0.01$, and acoustic time step off-centering of $\beta = 0.1$.

Figure 3 shows contours of u and w velocity at $t = 10000 \text{ s}$, with results using terrain-following coordinates on top, and those using IBM below. In the analytical solution there is no interaction with the topography, and the velocity field is specified by equation 4 at all times. When terrain-following coordinates are used it is clear that the distortion of the grid makes it impossible to isolate the flow aloft from terrain effects. Waves, induced by errors in the coordinate transformation, form above the mountain range. Horizontal velocity should range from 0 to 10 m/s, and vertical velocity should remain zero. However, horizontal velocities of -5.8 to 14.1 m/s and vertical velocities greater than $\pm 4 \text{ m/s}$ are present. These errors are negligible in the IBM-WRF simulation. At the end of the simulation, horizontal velocity ranges between -0.04 and 10.08 m/s, and vertical velocity between -0.04 and 0.06 m/s.

Snapshots of the scalar cloud are included in figure 4, along with the associated errors. Three different times ($t = 0, 5000, \text{ and } 10000 \text{ s}$) are depicted as the scalar advects from right to left in the domain. Significant distortion of the scalar anomaly occurs as it advects over the terrain features in the simulation with sigma coordinates. At the last time the shape of the cloud is not only distorted, but the center has advected 4.5 km less than in the analytical solution. Error is calculated as the difference between the numerical and analytical solution, and is shown with contour intervals of 0.01. At the last time shown, error ranges between -0.766 and 0.673. These errors are on the order of the analytical scalar concentration, which ranges from 0 to 1, indicating large errors arising from the use of sigma coordinates. In the simulation using the immersed boundary method, distortion of the cloud is eliminated. No contours appear in the IBM-WRF error plot, because the error is less than the threshold of the first contour (0.01). Errors in the IBM-WRF simulation are included in figure 5 with appropriate contour levels. In IBM-WRF the deviation from the analytical solution ranges from -0.002 to 0.002. Contour intervals are 0.0005. The results of these simulations indicate that the truncation error is dominated by the term arising from the transformation to terrain-following coordinates, and errors from the pressure coordinate transformation and the finite

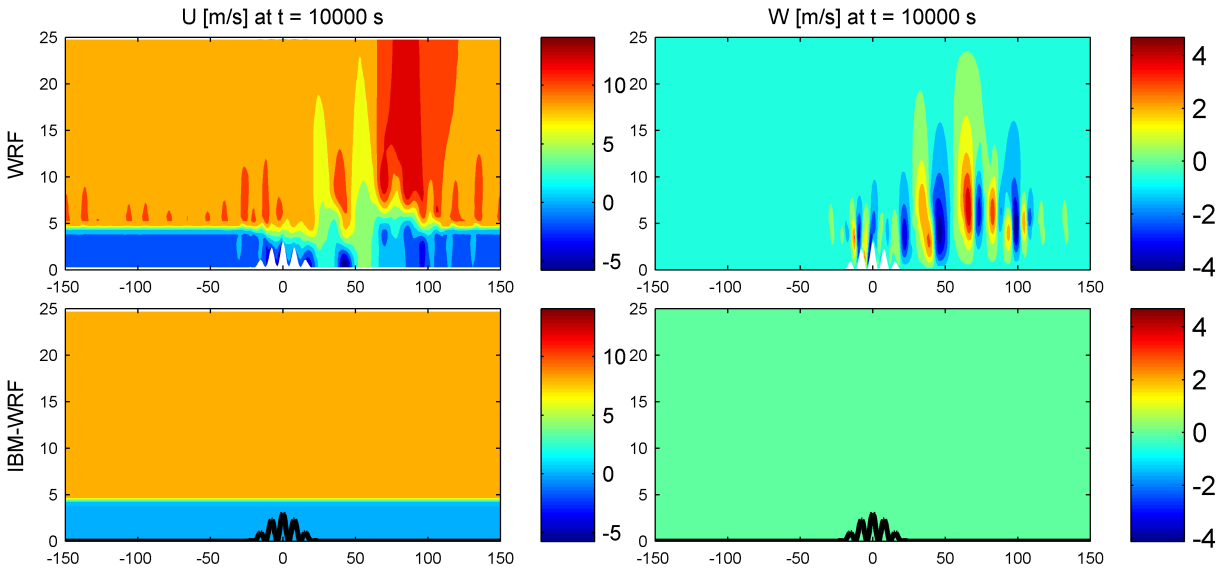


Figure 3: Contours of the u and w components of velocity in m/s for terrain-following coordinates (top) and the immersed boundary method (bottom) at $t = 10000$ s. Analytically, the velocity should equal the initial sounding throughout the duration of the simulation. Axes indicate domain size in km, and are not to scale.

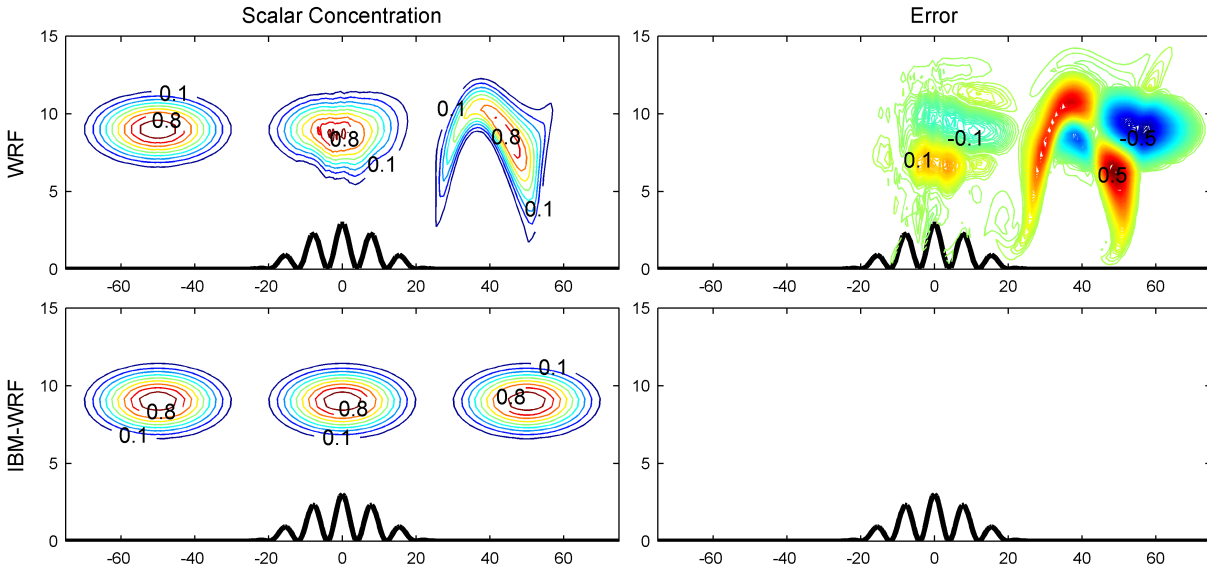


Figure 4: On the left, the scalar concentration is shown at $t = 0, 5000$, and 10000 s. Scalar units are non-dimensional with a range of 0 to 1. Contour intervals are in 0.1 increments. Error is shown on the right, and is calculated as the difference between the numerical and analytical solutions. Contour intervals are 0.01. The zero contour is suppressed. Axes indicate domain size in km, and are not to scale.

Table 1: Summary of errors at $t = 10000$ s for the WRF simulations with the default advection scheme and those presented in Schär et al. [2002]. Analytical values of φ_{min} and φ_{max} are 0 and 1. $\Delta\varphi$ is the difference between the numerical and analytical solutions.

Coordinate	Order of Advection Scheme	φ		$\Delta\varphi$	
		min	max	min	max
WRF Sigma	h:5 th , v:3 rd	-0.039	0.856	-0.766	0.673
IBM-WRF	h:5 th , v:3 rd	-0.002	0.992	-0.002	0.002
Schär et al. Sigma	1 st	0.000	0.284	-0.700	0.213
	2 nd	-0.168	0.953	-0.174	0.162
	4 th	-0.058	1.001	-0.057	0.052
Schär et al. No Topography	1 st	0.000	0.762	-0.220	0.141
	2 nd	-0.023	0.985	-0.023	0.021
	4 th	-0.002	0.984	-0.002	0.002

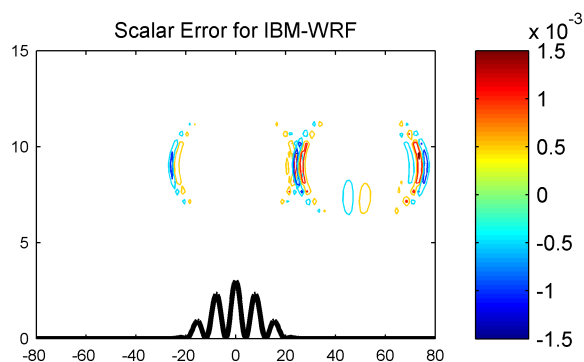


Figure 5: Error is shown for the immersed boundary method case at $t = 0, 5000,$ and 10000 s. Contour intervals are 0.0005. The zero contour is suppressed. Axes indicate domain size in km, and are not to scale.

differencing scheme are negligible.

A comparison of the WRF and IBM-WRF results and those presented in Schär et al. [2002] is included in table 1. Schär et al. published results for simulations with 1st, 2nd, and 4th order advection schemes (among others which are not included here). For reference, Schär et al. also included a set of simulations with no topography. Error in the reference simulations is exclusively caused by the finite differencing schemes. As expected, higher order advection schemes decrease error for both sigma coordinates and the reference cases of Schär et al.. The IBM-WRF simulation performs as well or better than the 4th order reference case with no topography. This is a logical result, as the immersed boundary method alleviates the need for a coordinate transformation and the simulation is of a similar order. WRF with sigma coordinates

produces more errors than expected. Despite the higher order scheme, WRF does not perform as well as the 2nd order sigma case of Schär et al. The main difference between the simulations is that the wind is prescribed in Schär et al., but solved for in the WRF simulations. This is a large difference in the models, and probably accounts for the larger errors in the WRF simulations. It is important to note then that IBM-WRF correctly evaluates the flow field and transport of the scalar cloud.

Schär et al. cite several causes of error in the idealized advection tests, first reasoning that “Schemes with implicit diffusion suffer particularly large coordinate transformation errors. Diffusion spreads out the solution in computational space, rapidly broadens the initial anomaly, and thereby makes the scheme more susceptible to coordinate transformations.” In a grid refinement study, Schär et al. found that the solution was extremely sensitive to horizontal resolution, and large gains in accuracy could be achieved through increased horizontal resolution. The solution was shown to be insensitive to vertical resolution. Additionally, as shown in table 1, Schär et al. found that increasing the order of the advection scheme had a beneficial impact on the quality of the solution. Accuracy was largely gained from an increase in the order of the horizontal scheme, whereas the vertical scheme had little effect. These possible causes of error are investigated in the following section.

4 ANALYSIS OF TRUNCATION ERRORS

Schär et al. [2002] carried out a theoretical analysis of truncation errors in the transformed coordinate. The analysis considers the one-dimensional scalar advection equation. After deriving the truncation er-

Table 2: Summary of errors at $t = 10000$ s for the WRF and IBM-WRF simulations with advection schemes of increasing order. Analytical values of φ_{min} and φ_{max} are 0 and 1. $\Delta\varphi$ is the difference between the numerical and analytical solutions.

Coordinate	Order of Advection Scheme	φ		$\Delta\varphi$	
		min	max	min	max
WRF Sigma	3 rd	-0.028	0.735	-0.746	0.480
	4 th	-0.373	0.885	-1.073	0.867
	5 th	-0.064	0.893	-0.857	0.852
	6 th	-0.439	1.325	-1.050	0.820
IBM-WRF	3 rd	-0.004	0.991	-0.004	0.005
	4 th	-0.003	0.992	-0.003	0.003
	5 th	-0.002	0.992	-0.002	0.002
	6 th	-0.002	0.992	-0.002	0.001

ror with a Taylor series expansion, it may be split into two parts. E_{fd} is attributed to the finite differencing scheme, and E_t to the coordinate transformation. Errors are given in 6 for a first order upwind scheme.

$$E_{fd} = \frac{\Delta x}{2} \frac{\partial}{\partial x} \left(u \frac{\partial \varphi}{\partial x} \right) + O(\Delta x^2) \quad (6a)$$

$$E_t = -\frac{\Delta x}{2} u \frac{\partial \varphi}{\partial x} J^{-1} \frac{\partial J}{\partial x} + O(\Delta x^2) \quad (6b)$$

It is seen here that the leading term for the error due to each cause is of the same order of magnitude (Δx). Large Jacobian terms as well as large gradients in the Jacobian lead to significant increases in the transformation truncation error. In the limit of the Jacobian approaching zero, the truncation error reduces to the theoretical form from the finite differencing scheme.

In this section the effects of the advection scheme, horizontal and vertical resolution, and terrain slope are studied. It is shown that the error produced by the finite differencing scheme is negligible in comparison to the error caused by the coordinate transformation used in WRF.

4.1 EFFECT OF ADVECTION SCHEME

Schär et al. noted that even order advection schemes produced better results than odd order schemes with implicit diffusion. As the default scheme in WRF is an odd order, it was initially thought that the even order scheme would produce less error. The effects of the advection scheme are presented here, where each available option is tested in WRF. For comparison, simulations are included with both terrain-following coordinates and the immersed boundary method.

Table 2 includes the error for each advection scheme with each type of coordinate (sigma and IBM). It can be seen here that in WRF with sigma coordinates odd order advection schemes produce less error than even order schemes, although the accuracy of both types is poor. Additionally, it is not clearly beneficial to increase the order of the advection scheme when the native WRF coordinate is used in this test case example. Both of these results are contrary to the findings of Schär et al. In contrast to the large errors produced with sigma coordinates, errors in the IBM-WRF simulations are extremely small. With IBM it is clear that the solution benefits from increasing the order of the advection scheme. A preference is not shown for even or odd advection schemes in the simulations using IBM. For comparison, simulations in WRF with no topography yielded almost identical results to those with IBM. As found in the results with default settings, truncation error due to the finite differencing scheme is negligible in comparison to that of the coordinate transformation.

Figure 6 gives insight into the behavior of odd and even order advection schemes when used with the sigma coordinate in WRF. This figure depicts the scalar anomaly at three instances in time, along with error contours for each of the instances. The 3rd order advection scheme is shown in the top figures, with a 4th order scheme used in the figures below. The odd order scheme is upwind biased and implicitly diffusive. As the scalar advects over the peaks in the terrain, significant distortion of the cloud occurs. The implicit diffusion seems to be beneficial, in that it allows the cloud to remain a cohesive mass. In the even order scheme the scalar cloud disperses as it advects over the terrain. This leads to large errors in the location of the cloud,

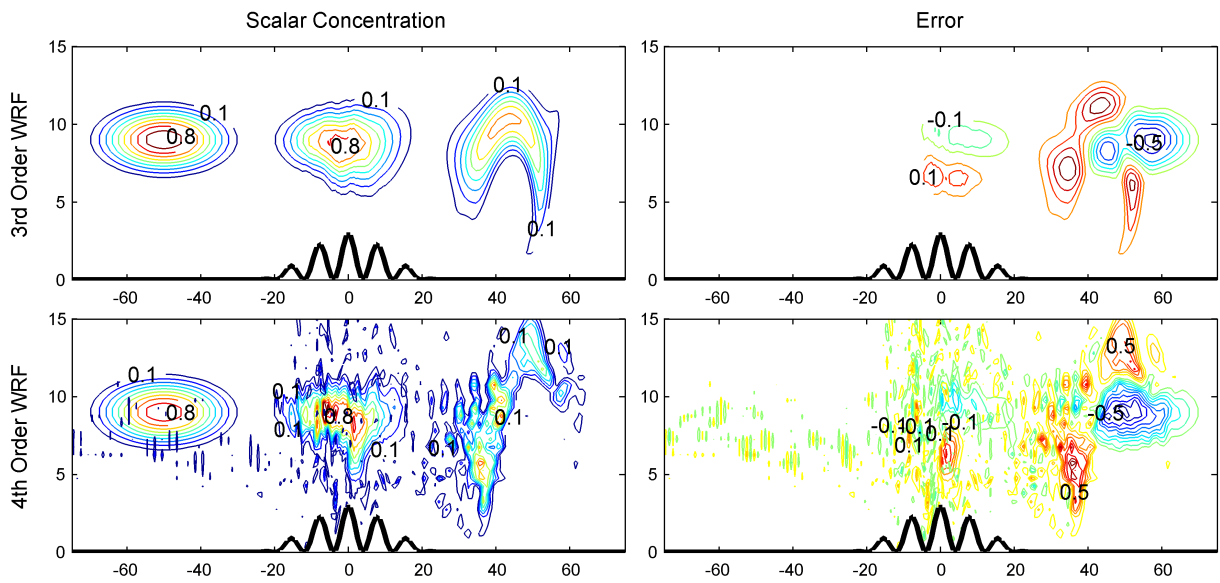


Figure 6: As in figure 4, but with error contour increments of 0.1. 3rd and 4th order advection schemes are used in a WRF simulation with terrain-following coordinates.

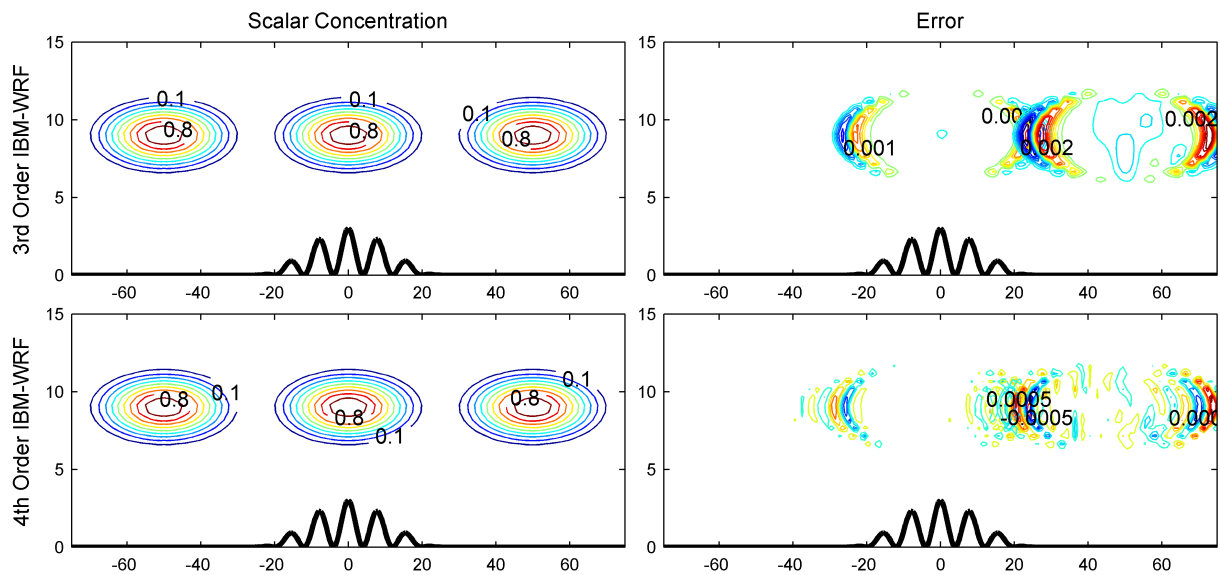


Figure 7: As in figure 4, but with error contour increments of 0.0005. 3rd and 4th order advection schemes are used in a WRF simulation with the immersed boundary method.

Table 3: Summary of errors at $t = 10000$ s for WRF simulations with sigma coordinates at various spatial resolutions. The default advection scheme is used (5th order horizontal and 3rd order vertical).

Δx (m)	Δz (m)	φ		$\Delta\varphi$	
		min	max	min	max
1000	500	-0.039	0.856	-0.766	0.673
1000	250	-0.128	0.897	-1.040	0.897
1500	500	-0.071	0.699	-0.832	0.588
500	500	-0.030	0.300	-0.983	0.300

as well as significant magnitudes of negative scalar concentration.

Figure 7 provides the same information for simulations where IBM is used. In this case the odd and even order advection schemes produce accurate results with similar error magnitudes. While one scheme is diffusive and the other is dispersive, the effect of these errors are not obvious in the solution. The results illustrate that a vast improvement in the solution can be achieved using IBM to eliminate the need for the terrain-following change of coordinate.

4.2 EFFECT OF SPATIAL RESOLUTION

Schär et al. found that significant improvements in accuracy could be achieved through increasing horizontal resolution, while sensitivity to vertical resolution was limited. In fact, it was noted that increasing the resolution from $\Delta x = 1000$ m to $\Delta x = 500$ m reduced the error from 21% to 4%, while decreasing the resolution to $\Delta x = 1500$ m led to 78% error.

The effects of spatial resolution are examined in WRF using the default advection scheme. The results of the base case along with three additional simulations are presented in table 3. First, vertical resolution was increased from $\Delta z = 500$ m to $\Delta z = 250$ m. In the next two simulations, horizontal resolutions of $\Delta x = 1500$ m and $\Delta x = 1000$ m are used. Unlike in the Schär et al. results, it is not clearly beneficial to increase the resolution. In fact, the solution deteriorated more by increasing the horizontal resolution from $\Delta x = 1000$ m to $\Delta x = 500$ m, than it deteriorated from decreasing the resolution to $\Delta x = 1500$ m. The solution also deteriorated with increased vertical resolution. In conclusion, the errors in these simulations are so large that doubling the number of grid points in a dimension does not lead to smaller error. It is possible that additional grid refinement would help, but this is beyond the scope of this study. In contrast, IBM-WRF produces an accurate solution without the need for additional resolution.

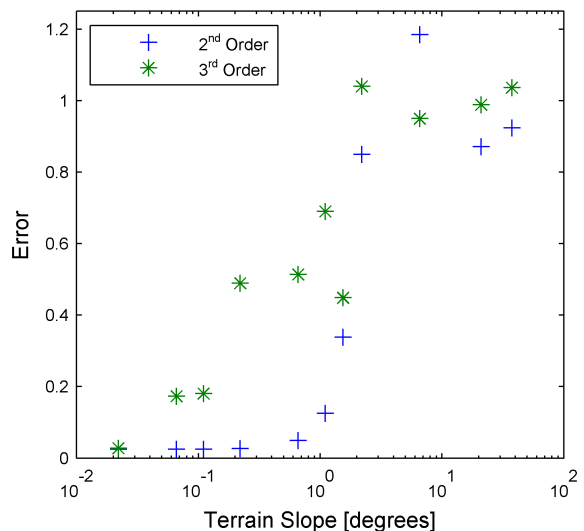


Figure 8: Error is plotted as a function of terrain slope for simulations with 2nd and 3rd order advection schemes.

4.3 EFFECT OF COORDINATE TRANSFORMATION

The effect of the magnitude of the Jacobian on the accuracy of the solution is evaluated with a series of simulations with decreasing terrain height. In these simulations the terrain is still defined by equation 3, but the maximum amplitude of the terrain h_o ranges from 0 to 3000 m. The half width of the terrain is held constant. This results in a maximum terrain slope that ranges from 0 degrees to 49 degrees, when a 3000 m peak height is used. Analytically the solution for the scalar cloud should be independent of the terrain because it is isolated by the inviscid shear layer. Therefore, decreasing the terrain height affects the solution aloft by decreasing the grid distortion aloft caused by the terrain-following coordinate.

Results are presented in figure 8 for simulations with 2nd and 3rd order advection schemes. In this

plot error is defined by equation 7.

$$E = \max |\varphi_{numerical} - \varphi_{analytical}| \quad (7)$$

It can be seen in this plot that error grows quickly with increasing terrain slope. In fact, a slope of just one degree will cause error of over 10% with the 2nd order scheme, and almost 70% with the 3rd order scheme. Beyond a one degree slope the error is very large regardless of the advection scheme.

Large errors are produced when the grid is not orthogonal in the region of the shear velocity layer. A very small coordinate slope in this region will lead to large truncation errors in the velocity field. This induces a wave in the flow, as was shown in figure 3, with a wavelength on the order of that specified in the equation for the terrain. The point here is that even with shallow terrain slopes the truncation error can have devastating effects on the accuracy of the solution when large gradients and discontinuities exist in the flow field.

5 CONCLUSIONS

This work has demonstrated that the immersed boundary method is an effective tool not only for representing the complex terrain boundary, but also for eliminating errors far from the boundary caused by the terrain-following coordinate transformation. An idealized advection test was used to illustrate the effectiveness of the immersed boundary method in eliminating the errors associated with terrain-following coordinates. Error in the simulations with sigma coordinates could not be reduced to the level of error in the IBM simulations. Attempts were made to decrease error in simulations with the sigma coordinate, by increasing the order of the finite difference scheme, refining the grid resolution, and even reducing the terrain slope. Ultimately the IBM-WRF simulations reproduced the analytical solution with the highest accuracy.

6 ACKNOWLEDGEMENTS

The authors are grateful for the support of a Lawrence Scholars Program Fellowship from Lawrence Livermore National Laboratory (LLNL). This project was partially funded by the LLNL Laboratory-Driven Research and Development program. The support of National Science Foundation Grant ATM-0645784 [FKC] (Physical Meteorology Program: S. Nelson, Program Director) is also gratefully acknowledged. This work was performed

under the auspices of the U.S. Department of Energy by Lawrence Livermore National Laboratory under Contract DE-AC52-07NA27344.

REFERENCES

- A. Adcroft, C. Hill, and J. Marshall. Representation of topography by shaved cells in a height coordinate ocean model. *Mon. Weather Rev.*, 125:2293–2315, September 1997.
- T. Gal-Chen and R.C.J. Somerville. On the use of a coordinate transformation for the solution of the navier-stokes equations. *J. Comp. Phys.*, 17:209–228, 1975.
- J.B. Klemp, W.C. Skamarock, and O. Fuhrer. Numerical consistency of metric terms in terrain-following coordinates. *Mon. Weather Rev.*, 131:1229–1239, July 2003.
- J.B. Klemp, W.C. Skamarock, and J. Dudhia. Conservative split-explicit time integration methods for the compressible nonhydrostatic equations. *Mon. Weather Rev.*, 135:2897–2913, August 2007.
- K.A. Lundquist, F.K. Chow, J.K. Lundquist, and J.D. Mirocha. Development of an immersed boundary method to resolve complex terrain in the weather research and forecasting model. In *7th Symposium on the Urban Environment*. American Meteorological Society, 2007.
- K.A. Lundquist, F.K. Chow, J.K. Lundquist, and J.D. Mirocha. Imposing land-surface fluxes at an immersed boundary for improved simulations of atmospheric flow over complex terrain. In *18th Symposium on Boundary Layers and Turbulence*. American Meteorological Society, 2008.
- J. Mohd-Yusof. Combined immersed boundary/b-spline methods for simulations of flow in complex geometry. Technical report, Center for Turbulence Research, NASA Ames/Stanford Univ., Palo Alto, CA, 1997.
- N.A. Phillips. A coordinate system having some special advantages for numerical forecasting. *J. Meteor.*, 14:184–185, April 1957.
- C. Schär, D. Leuenberger, O. Fuhrer, D. Lüthi, and C. Girard. A new terrain-following vertical coordinate formulation for atmospheric prediction models. *Mon. Weather Rev.*, 130:2459–2480, October 2002.
- W.C. Skamarock, J.B. Klemp, J. Dudhia, D.O. Gill, D.M. Barker, W. Wang, and J.G. Powers. A description of the advanced research WRF version 2. Technical Report NCAR/TN-468+STR, National Center for Atmospheric Research, Boulder, CO, June 2005.